heritage

MDPI

Article

Correlation of Visible Reflectance Spectrometry and Portable Raman Data for Red Pigment Identification

Anna M. Gueli [1], Rosaria Galvagno [1], Adriana Incardona [1], Eleonora Pappalardo [2], Giuseppe Politi [1], Giuseppe Paladini [1,*] and Giuseppe Stella [1]

[1] Department of Physics and Astronomy "Ettore Majorana", University of Catania, Via S. Sofia 64, Catania 95123, Italy; anna.gueli@unict.it (A.M.G.); rosaria.galvagno@phd.unict.it (R.G.); adriana.incardona@phd.unict.it (A.I.); giuseppe.politi@ct.infn.it (G.P.); giuseppe.stella@dfa.unict.it (G.S.)

[2] Department of Educational Sciences, University of Catania, Via Teatro Greco 84, Catania 95124, Italy; eleonora.pappalardo@unict.it

* Correspondence: giuseppe.paladini@dfa.unict.it

Abstract: The accurate identification of pigments is of principal relevance in the field of cultural heritage conservation and restoration practices. In this preliminary study, a first attempt to set up a procedure for accurate red pigment identification, based on the assessment of the correlations existing between visible reflectance spectrometry (vis-RS) and Raman data, is presented. The proposed approach involved the realization of a library consisting of data acquired on a set of 35 pure red historical pigments supplied by ©*Kremer Pigmente*. In particular, vis-RS data, collected through a Konica Minolta CM-2600d spectrophotometer, were registered, together with the position of the Extrema Points (E.P.s) encompassing both the maximum and minimum points of the first derivative of the % spectral reflectance factor (SRF%) curves. Portable Raman spectroscopy measurements were collected by a B&W Tek Inc. portable Raman spectrometer equipped with a 785 nm laser. For each tested pigment, the positions and relative intensities of the characteristic Raman peaks were considered. The library was then tested for the characterization of the red/reddish painted areas of the medieval wall painting located within *The Norman Castle of Aci Castello* (Catania, Italy), and was shown to be essential for the unambiguous identification of the pigment used. It is worth noting that this study represents the first novel attempt to establish a reliable and efficient methodology for pigment identification, offering promising prospects in reducing uncertainties and ambiguities arising from the application of a single stand-alone approach.

Keywords: pigments identification; library; visible reflectance spectrometry; portable Raman spectroscopy; wall painting

Citation: Gueli, A.M.; Galvagno, R.; Incardona, A.; Pappalardo, E.; Politi, G.; Paladini, G.; Stella, G. Correlation of Visible Reflectance Spectrometry and Portable Raman Data for Red Pigment Identification. *Heritage* **2024**, *7*, 2161–2177. https://doi.org/10.3390/heritage7040102

Academic Editors: Manuela Vagnini, Chiara Anselmi, Francesca Volpi and Vittoria Guglielmi

Received: 5 January 2024
Revised: 26 March 2024
Accepted: 4 April 2024
Published: 6 April 2024

1. Introduction

The accurate identification of pigments, through the employment of a combination of advanced analytical techniques and interdisciplinary collaborations, provides insights into the understanding of an artist's creative process and helps in finding solutions to art historical research questions, including conservation, restoration, and authentication [1–7]. In fact, it enables restorers to authentically preserve the original intentions of artists, while enhancing our comprehension of historical techniques and cultural contexts. This process sheds light on the evolution of artistic practices and materials, tracing the development of pigments from ancient civilizations to modern times. Over the recent years, much interest has been notably directed towards the development of methodologies and novel strategies aimed at the comprehensive characterization of historical inorganic/organic pigmenting agents, alongside the identification of possible degradation products originating from the interaction of such agents with the surrounding environment [8–16]. These aspects play a fundamental role not only in estimating the choice and style of the artist but also in reproducing similar materials in accordance with ancient recipes which

can be used for restoration interventions [17–24]. As is well known, the preservation and conservation of pigmented artworks generally require the employment of techniques that provide valuable information while minimizing the potential risk of damage. In this sense, a good strategy consists of the use of complementary non-invasive or, at least, micro-destructive methodologies able to perform in situ measurements with portable equipment that ensures the acquisition of useful data in conservation and restoration programs [25–28]. In this context, non-destructive techniques such as diffuse reflectance spectrometry, operating in the visible range (vis-RS) [29–31], and portable Raman spectroscopy [32–37] have proved to be essential and easily accessible for the assessment of various components in paintings [38]. In particular, since the beginning of the twenty-first century, *vis-RS* has become pivotal in the study of cultural heritage materials, i.e., in the ability to potentially discriminate both organic/inorganic materials [39,40], in the direct analysis of color discoloration on surfaces, as well as for the validation test of novel protective and cleaning consolidant products to be applied for conservation and preservation purposes. Notably, the reflection spectrum of a pigment has a behavior that strongly depends on the particle size, suspending medium, and refractive index of the investigated sample [41,42]. Nowadays, the ability to collect the reflectance contribution originating from small surface areas, in conjunction with easy-to-use, portable, and low-cost features, makes such methodology appealing in the characterization of artwork pure pigments [43]. Additionally, Raman spectroscopy has been largely utilized in the study of the molecular composition of pigment mixtures in paintings [13,44,45], ceramics [46–48], manuscripts [49,50], and wall paintings [51,52]. However, it is worth remarking that, in most cases, the presence of ground materials and binding agents, typically made up of organic-based compounds, is responsible for the onset of a high fluorescence background which may cover the weak Raman signal emitted by the pigment, making its identification a very challenging task. Currently, portable Raman spectrometers are commercially available. Despite the beneficial cost-effectiveness and user-friendly properties of portable instruments, which make them particularly appealing, their spectral resolution and signal-to-noise ratio cannot be compared with those of typical benchtop settings [53]. Nevertheless, the management of immovable objects of high artistic–historical value, i.e., frescoes and wall paintings, makes the employment of portable Raman instruments a fundamental requirement for their proper characterization [26,54–57] due to bureaucratic difficulties in relocating/transferring the artwork from the site to the laboratory. Whether using either vis-RS or portable Raman, the identification of the pigment "fingerprint" utilized in colored artworks may be challenging, especially for the characterization of objects affected by a poor preservation state. Accordingly, all measurement surveys should always be accompanied by a detailed comparison with a proper database for a feasible and unambiguous identification process. In this context, this paper mainly focuses on the description of an approach for accurate red pigment identification based on the association of the obtained data with those supplied by a home-made database containing vis-RS and portable Raman data of 35 pure red historical pigments provided by ©*Kremer Pigmente* (GmbH & Co. KG (Aichstetten, Germany)), achieved through the employment of portable instrumentations usable in situ. The aim was to establish a comprehensive repository capable of streamlining the red pigment identification process directly in the field, starting from a systematic comparison of the reference dataset with those achieved in a real context. This is extremely useful in all those cases in which unexpected challenges, such as instrumental issues, sample limitations, or ambiguous results, can impede a conclusive and reliable pigment recognition. In particular, the first step was devoted to the realization of a database consisting of integrated *vis-RS* and portable Raman data aimed at identifying potential "smart markers", defined as a single, or an ensemble, of potential values/data characteristic of the sample which could serve as a strategical indicator for correlation analysis, thus enabling its insightful and unambiguous identification. The constructed database was then tested for the in situ multi-technique characterization of the red areas of a wall painting within The Norman Castle of Aci Castello (Catania, Italy), representing Mary with child, with the aim to

validate and establish a reliable and efficient approach to pigment identification. Specifically, the state of preservation of the wall painting does not allow an easy reconstruction of the represented subject. No specific studies have been devoted to its analysis and no information about its existence inside the castle is available in the historical sources.

A further objective of this work is the improvement of the database of historical pigments available at the PH3DRA (PHysics for Dating Diagnostics Dosimetry Research and Applications) labs, in terms of vis-RS and portable Raman data, in agreement with the goals set in a previously published paper by some of the authors [58,59].

2. Materials and Methods

2.1. Materials

2.1.1. Red Pigments Used for Library

The set of pigments used for this study, composed of 35 powdered samples supplied in 3 mL containers, was purchased from ©*Kremer Pigmente* (Germany). The commercial names and reference numbers are specified in Table 1. The reference materials were studied without any further treatment. The examined set includes both pigments used in the past centuries, such as cinnabar (ID codes: 10620, 10621 and 10622), madder lake (ID code: 37202), and ochres (ID codes: 11574, 11575, 11576, 11577, 11584 and 11585), as well as modern and contemporary ones, i.e., alizarine (ID code: 23610) and carmine naccarat (ID code: 42100).

Table 1. Identification code, color index, product name, and a brief description of the red pigments used in this paper (provided by the sales company).

ID Code	Color Index	Product Name	Description
23610	PR 83	Alizarine crimson dark	Synthetic organic pigment
42100	NR 4.1, 75470	Carmine naccarat	Natural aluminum lake of carminic acid
10800	PY 39. 77085	Realgar	Natural orange-red sulphide of arsenic
42500	PR 105 77578	Red lead, minium	Synthetic Pb-based pigment
48700	PR 102	Caput Mortuum reddish	Natural iron oxide pigment
11300	PW 27.77811	Red jasper	Natural amorphous quartz
48120	PR 101.77491	Iron oxide red 120 m	Synthetic iron oxide pigment
40440	PBr 7	Pompei red	Synthetic iron oxide pigment
40351	PR 102.77491	Red mine ochre	Natural iron oxide pigment
40490	PR 102	Satorius red	Natural iron oxide pigment
40500	PR 102	Red bolus	Natural iron oxide pigment
40510	PR 102	Venetian red	Natural iron oxide pigment
40542	PR 101	English red light	Synthetic iron oxide pigment
40545	PR 101	English red deep	Synthetic iron oxide pigment
11574	PR 102	Burgundy red ochre medium, 0-80 μ	Natural iron oxide pigment
11575	PR 101.77491	Burgundy red ochre medium 0-120 μ	Synthetic iron oxide pigment
11576	PR 102	Burgundy red ochre deep 0-80 μ	Natural iron oxide pigment
11577	PR 101.77491	Burgundy red ochre deep 0-120 μ	Synthetic iron oxide pigment
11584	PR 102	Spanish red ochre 0-120 μ	Natural iron oxide pigment
11585	PR 102	Spanish red ochre 0-63 μ	Natural iron oxide pigment
48600	PR101	Iron oxide red natural	Synthetic iron oxide pigment
11360	PR102	Brown-red slate	Natural iron oxide pigment
48100	PR 101.77491	Iron oxide red 110 m, light	Synthetic iron oxide pigment
48150	PR 101.77491	Iron oxide red 130 b, medium	Synthetic iron oxide pigment
48200	PR 101.77491	Iron oxide red 130 m, medium	Synthetic iron oxide pigment
48250	PR 101.77491	Iron oxide red 222, dark	Synthetic iron oxide pigment
52350	PR 102. 77491	Translucent orange-red	Natural iron oxide pigment

52400	PR 101.77491	Translucent red medium	Synthetic iron oxide pigment
10620	PR 106. 77766	Natural cinnabar	Natural HgS mineral mercuric sulfide
10621	PR 106. 77766	Natural cinnabar, light	Natural HgS mineral mercuric sulfide
10622	PR 106. 77766	Natural cinnabar, powder	Natural HgS mineral mercuric sulfide
37000	NR 31	Dragon's blood, powder	Natural organic pigment
37202	NR 9. 75330	Madder lake	Natural organic pigment
36020	NR 25.75450	Lac dye	Natural organic pigment
37030	NO 2.75310	Resina kamala	Natural organic pigment

2.1.2. Wall Painting Located within the Norman Castle of Aci Castello (Catania, Italy)

Few traces of a wall painting survive inside a long rectangular room of the Castle, named "Byzantine Chapel", but, chronologically consistent with the rest of the building, no traces of Byzantine architecture survive. As said above, no specific analysis was carried out on the wall painting, whose state of preservation makes the complete reading of the scene and the style particularly difficult. Traces of a seated subject survive, evidently Mary, bearing a small naked figure on her legs, Christ. Evanescent traces of a third figure, a Saint, are preserved to the right, while, on the left, the painting is too damaged. Mary wears a red dress and a black-bluish mantle. A light pink-yellowish color, at some points converting into white, is used for naked portions of the figures: the hand for Mary and the legs for Jesus. The scene is framed by a thin red rim.

A total of 10 different areas of the wall painting were analyzed in situ, representative of red finishing layers (R#, with # = 1, …, 10), as summarized in Table 2 and indicated in Figure 1.

Table 2. Description of the investigated areas with the position within the wall painting.

Analyzed Area	Description	Figure
R1	Light-red area	not assignable to any figure
R2	Dark-red area	not assignable to any figure
R3	Dark-red area	not assignable to any figure
R4	Red area	not assignable to any figure
R5	Red area	halo of Mary
R6	Red area	not assignable to any figure
R7	Red area	not assignable to any figure
R8	Light-red area	not assignable to any figure
R9	Red area	not assignable to any figure
R10	Light-red area	not assignable to any figure

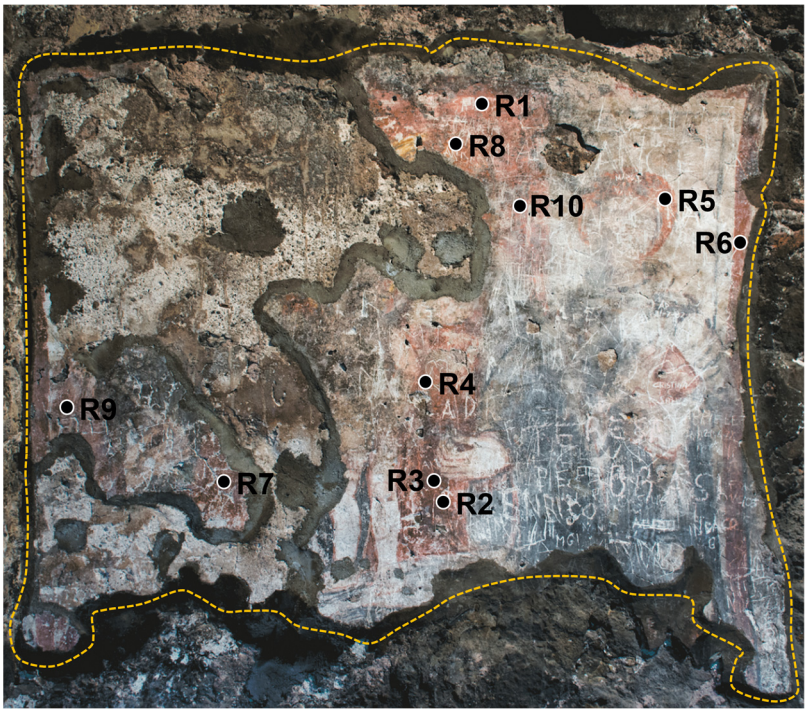

Figure 1. Investigated polychrome wall painting located within The Norman Castle of Aci Castello (Catania, Italy), with an indication of the analyzed areas. The yellow-dashed line indicates the painted area. The surface area is ~2 m^2.

2.2. Methods

2.2.1. Visible Reflectance Spectrometry (Vis-RS) Measurements

Vis-RS measurements were carried out by a Konica Minolta® model CM-2600d spectrophotometer (Konica Minolta, Tokyo, Japan), working in the 360–740 nm spectral range with a 10 nm acquisition step. The measurement geometry was d/8°, and the chosen measured area was 6 mm in diameter (SAV condition). The light provided by a Xenon lamp was diffused through an integrating sphere, uniformly illuminating the specimen. The light reflected by the sample then reached the optical system, where it was split into 10 nm-pitch components each processed by an analog processing circuit for the detection. In our case, a white calibration plate (CM-A145) and a black box (Zero-Calibration Box CM-A32 Minolta) were employed to perform the scale adjustment, as targets for the maximum and minimum lightness values [60]. The data elaboration, regarding SPEX/100 values (*SPecular component EXcluded and UV included*), was performed by dedicated software (SpectraMagic®, ver. 3.6), while the Origin® software (OriginPro 8) was used for data processing. The mean values for all data were obtained from three measurements, together with their respective uncertainties. The total uncertainty was then calculated using uncertainty propagation theory, which involves the square root of the sum of the squared standard deviation and the instrumental error. In particular, the instrumental error was evaluated considering the L*a*b* coordinates of the white calibration plate related to the 2° standard observer and D65 standard illuminant after the adjustment procedure.

The analysis involved first the behavior of the spectral reflectance factor (SRF%), accounting for the reflected/incident intensity percentage ratio, in the 400–700 nm range. Then, from the first derivative curves d(SRF%) of the spectral trends, the Extrema Points (E.P.s) related to the maximum, minimum, and inflection points were registered following the methodology proposed by Bacci et al. [39,61–63]. In particular, the high (absolute maxima, p-h) and low (relative maxima, p-l) peaks were recorded, together with the positions of valleys (absolute/relative minima, v) and shoulders (inflection points, sh).

For the evaluation of the derivative profiles, the Origin® software (OriginPro 8) was used, which performed, before the calculation of the first derivative, a smoothing on the

two preceding and two following points of the discrete data related to the SRF% curves using a third-degree polynomial function.

2.2.2. Raman Measurements

Raman measurements were performed, both for the realization of the laboratory database and for the in situ analysis, through a portable modular setup consisting of a BTC162E Glacier® T (B&W TEK Inc., Delaware, USA) high-resolution double pass transmission-based spectrometer (BTC162E), an FC-D-785 laser module (CNI, Changchun, China), and a lab-grade probe. The instrument is characterized by an excitation wavelength of 785 nm (diode laser), a 350 mW maximum laser excitation power, and a response-enhanced linear CCD detector (thermoelectric cooled, TE). The laser output power was continuously regulated in order to maximize the signal-to-noise ratio while avoiding thermal effects on the sample. For our measurements, the laser power was maintained at between 3% and 10% of the maximum power, corresponding to ~10.5–35 mW, depending on the specific sample. The spot size was 85 μm in diameter at a working distance of 5.5 mm. Spectra have been registered in the 60–3150 cm^{-1} wavenumber range, by using different acquisition times and a nominal resolution of ~5 cm^{-1}, adding several scans for each spectrum in order to improve the signal-to-noise ratio. Data elaboration, such as a baseline correction and a smoothing process, has been performed using the BWSpec 3.27 software.

3. Results and Discussion

3.1. Database Analysis Results

The proposed database involves the extraction of systematical information derived from the analysis of both the vis-RS and portable Raman data collected for each pigment within a limited range of wavelengths (i.e., visible) and using a single Raman excitation wavelength, respectively.

In Figure 2 we report, as an example, the Raman spectrum (Figure 2a) and the behavior of the SRF% (Figure 2b) together with the first derivative curve d(SRF%) vs. wavelength (Figure 2c) at SPEX/100 condition, obtained for sample ID code: 11300, red jasper, a glass-like transparency amorphous quartz, colored red by iron (III). This pigment was also rarely employed in historical painting layers [64] and in mosaics [65]. However, the selected sample was chosen mainly because it is particularly suitable for describing the database as it encompasses a wide range of different vis-RS and Raman features.

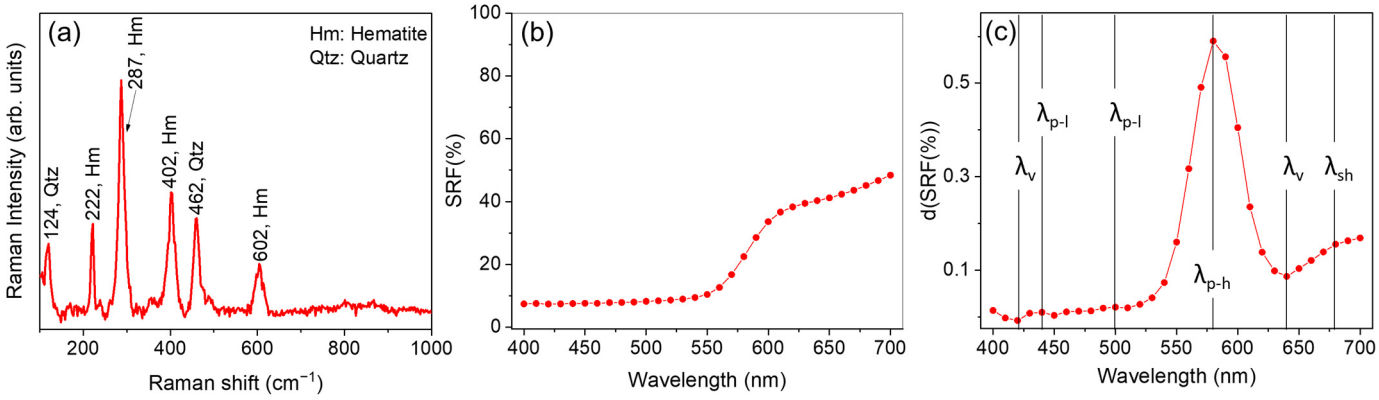

Figure 2. (a) Portable Raman spectrum, **(b)** spectral reflectance factor (SRF%), and (**c**) d(SRF(%)) curve obtained for sample ID code 11300—*Red jasper*.

It is worth noting that the CM2600d instrument has a high degree of accuracy and precision. In terms of SRF%, the relative percentage error obtained was <1%, considering the instrumental error and the average of the three measurements. Thus, the true uncertainty is related to the position of the peak of the first derivative, which is ±10 nm.

The detected Raman profile (Figure 2a) revealed, as main features, intense peaks at 222 cm^{-1} (A_{1g}), 287 cm^{-1} (E_g), 402 cm^{-1} (E_g), and 604 cm^{-1} (E_g), associated with ferric oxide (hematite, Fe_2O_3) [66], together with a contribution at 124 cm^{-1} and 462 cm^{-1} ascribable to quartz (SiO_2) [66].

In particular, the general consistency between the observed compositions retrieved for all the investigated red pigments with those warranted in the datasheets provided by the pigment manufacturer was verified by comparing the experimental data with both the relevant scientific literature [67–73] and the accessible online databases, IRUG [74] and RRuff [75]. In our case, the collected Raman spectra (see Figure 3) have revealed distinct fingerprint features, whose positions are listed in Table 3 together with their relative intensities, in compliance with the certified composition of the investigated set.

Table 3. Main Raman signals (wavenumber and relative intensity) and E.P. positions extracted from the analysis of the d(SRF(%)) vs. λ profiles associated with the 35 powdered red pigments supplied by ©*Kremer Pigmente*.

ID Code	Raman Features [1] (cm^{-1})	Extrema Points [2] (nm)
23610	1293 m, 1322 m, 1479 vs	430 (v); 480 (sh); 510 (sh); 620 (p-h); 680 (v)
42100	N/A	410 (sh); 440 (v); 480 (sh); 520 (p-l); 550 (v); 610 (p-h); 680 (p-l)
10800	140 m, 181 s, 191 s, 217 s, 252 m, 339 s, 351 vs	420 (v); 480 (sh); 560 (p-h); 650 (p-l); 680 (p-l)
42500	118 vs, 149 m, 222 w, 312 m, 389 m, 547 s	570 (p-h); 650 (sh); 690 (p-l)
48700	219 vs, 285 vs, 402 m, 483 w, 602 w	420 (v); 460 (v); 510 (sh); 590 (p-h); 640 (v); 680 (sh)
11300	120 s, 222 s, 287 vs, 402 s, 460 s, 604 s	420 (v); 440 (p-l); 500 (p-l); 580 (p-h); 640 (v); 680 (sh)
48120	219 vs, 287 vs, 402 m, 491 w, 604 w	430 (v); 450 (p-l); 590 (p-h); 640 (v); 690 (sh)
40440	287 w, 1194 br, 1282 br	440 (p-l); 460 (v); 510 (sh); 590 (p-h); 650 (v); 680 (w); 690 (sh)
40351	219 m, 287 s, 402 m, 604 w	410 (v); 440 (v); 510 (sh); 580 (p-h); 640 (v); 680 (sh)
40490	143 vs, 224 w, 290 m, 412 w, 605 w	410 (v); 470 (v); 580 (p-h); 650 (v)
40500	141 w, 290 w	420 (v); 440 (p-l); 590 (p-h); 680 (p-l)
40510	224 s, 289 vs, 411 s, 496 w, 609 w, 1008 m	500 (sh); 580 (p-h); 640 (v); 690 (sh)
40542	224 s, 290 vs, 1087 w	420 (v); 440 (sh); 590 (p-h), 650 (v); 690 (sh)
40545	224 s, 291 vs, 408 m, 496 s, 610 w, 1086 m	420 (v); 440 (sh); 480 (p-l); 590 (p-h); 640 (v); 690 (p-l)
11574	284 w	470 (v); 490 (p-l); 590 (p-h); 660 (v); 680 (p-l)
11575	284 w	430 (p-l); 490 (p-l); 590 (p-h); 660 (p-l); 680 (p-l)
11576	N/A	500 (sh); 590 (p-h); 650 (v); 680 (sh)
11577	N/A	410 (v); 450 (p-l); 490 (p-l); 590 (p-h); 660 (v); 680 (sh)
11584	224 w, 285 w	410 (v); 450 (p-l); 580 (p-h); 650 (v); 680 (p-l)
11585	224 w, 285 w	440 (p-l); 490 (p-l); 580 (p-h); 680 (sh)
48600	220 s, 291 vs, 408 m, 496 w, 610 w	420 (v); 500 (sh); 590 (p-h); 640 (v); 650 (p-l)
11360	284 w, 1130 w (br), 1228 s (br), 1288 s (br), 1428 s (br)	420 (v); 460 (p-l); 480 (v); 500 (p-l); 510 (p-l); 570 (p-h); 640 (v)
48100	219 s, 285 vs, 402 m, 493 w, 606 m	430 (v); 460 (v); 500 (sh); 590 (p-h); 640 (v); 680 (sh)
48150	222 vs, 287 vs, 404 m, 489 w, 606 m	420 (sh); 450 (v); 510 (sh); 590 (p-h); 640 (v); 670 (sh)
48200	222 vs, 287 vs, 404 m, 494 w, 606 m	490 (p-l); 510 (sh); 580 (p-h); 640 (v); 670 (sh)
48250	219 vs, 285 vs, 402 m, 485 w, 600 m	450(v); 510 (sh); 590 (p-h); 650 (v); 680 (sh)
52350	219 vs, 285 vs, 402 m, 484 w, 598 m	440 (p-l); 590 (p-h); 640 (v); 690 (p-l)
52400	219 w, 285 m, 400 m, 598 w	480 (p-l); 510 (sh); 600 (p-h); 650 (v); 690 (sh)
10620	250 vs, 280 m, 340 s	430 (p-l); 460 (p-l); 510 (sh); 600 (p-h); 680 (sh)
10621	252 vs, 280 m, 342 s	420 (v); 600 (p-h)
10622	252 vs, 283 m, 343 m	420 (sh); 470 (sh); 500 (sh); 530 (sh); 610 (p-h); 680 (sh)
37000	N/A	420 (sh); 460 (v); 560 (sh); 640 (p-h); 680 (sh)

37202	N/A	440 (p-l); 480 (sh); 510 (p-l); 530 (v); 620 (p-h)
36020	N/A	470 (sh); 520 (sh); 610 (p-h)
37030	N/A	410 (sh); 440 (p-l); 470 (p-l); 510 (sh); 630 (p-h); 680 (p-h)

[1] **vs**: very strong; **s**: strong; **m**: medium; **w**: weak; **sh**: shoulder; **br**: broad. [2] **p-h**: high peak; **p-l**: low peak; **v**: valley; **sh**: shoulder.

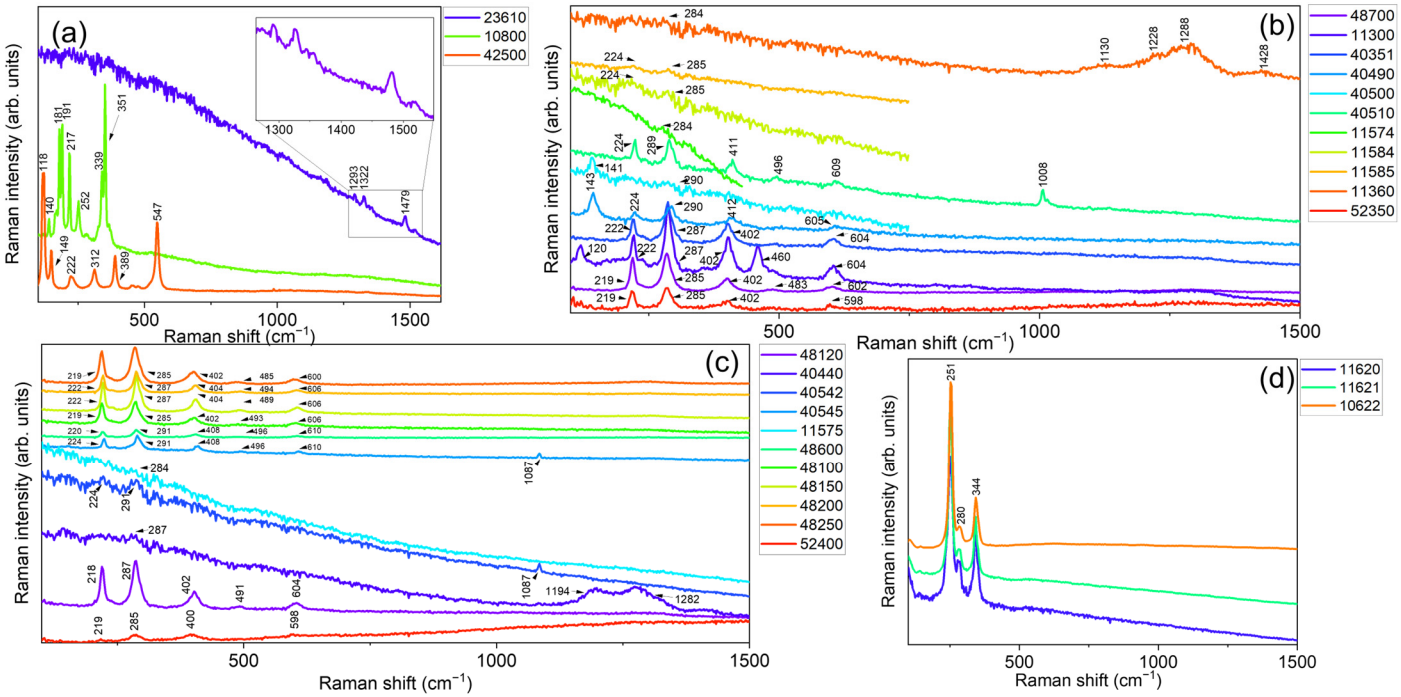

Figure 3. Measured portable Raman spectra of the 28 powdered samples reported in Table 3, using an excitation wavelength of 785 nm in the 100–1500 cm^{-1} spectral range. Spectra were vertically offset for clarity and divided into four different panels, respectively displaying measurements collected on: (**a**) three unique pigments based on organic (23610—*Alizarine crimson dark*), As-(10800—*Realgar*), and Pb-based (42500—*Red lead, minium*) compounds, (**b**) natural (color index: PR102) and (**c**) synthetic (color index: PR101) iron oxide-based pigments, and (**d**) Hg-based ones.

In more detail, the portable Raman spectra of the three unique pigments (See Figure 3a) based on organic (23610—*Alizarine crimson dark*), As-(10800—*Realgar*), and Pb-based (42500—*Red lead, minium*) compounds (See Tables 1 and 3) display the typical Raman signature of the components involved in the manufacture of the pigment, thus demonstrating uniform composition within the measurements. Red organic colors are typically challenging to analyze with the used set-up and excitation wavelength. Nevertheless, the portable Raman spectrum of 23610—*Alizarine crimson dark* (organic synthetic monoazo, naphthol) shows distinctive peaks at 1293 cm^{-1}, 1322 cm^{-1}, and 1479 cm^{-1}, despite a strong fluorescence background and low signal-to-noise ratio, allowing for its proper identification. Concerning sample 10800—*Realgar* (As_4S_4), major features at 140 cm^{-1}, 181 cm^{-1}, 191 cm^{-1}, 217 cm^{-1}, 252 cm^{-1}, 339 cm^{-1}, and 351 cm^{-1} can be easily distinguished, corresponding to the vibrational modes of the arsenic–sulfur bonds present in the compound, while, in the case of 42500—*Red lead, minium* (Pb_3O_4), a portable-Raman profile with characteristic peaks at 118 cm^{-1}, 149 cm^{-1}, 222 cm^{-1}, 312 cm^{-1} (lattice modes of the crystal structure) 389 cm^{-1}, and 547 cm^{-1} (stretching and bending vibrations of the Pb-O bonds) was observed, in agreement with the literature.

Going on, the comparison of the portable Raman spectra related to natural (color index: PR102) iron oxide-based pigments (Figure 3b) revealed an almost uniform composition based on iron(III) oxide–hematite, recognized by its typical stretching bands corresponding to the Fe–O bond centered at 222 cm^{-1} and 494 cm^{-1}, and deformation modes at 287 cm^{-1}, 402 cm^{-1}, and 604 cm^{-1}. A mixture of hematite and gypsum

($CaSO_4 \cdot 2H_2O$, main peak at 1008 cm^{-1}) was identified in the case of sample 40510—*Venetian* red, as expected by the well-known and certified composition of this pigment, while, in the case of sample 40490—*Satorius red* and 40500—*Red bolus*, a mixture of hematite and minium (lead(II,IV) oxide) can be recognized, besides the main vibrational bands of iron(III) oxide, with a contribution at 143 cm^{-1}. Finally, the portable Raman spectrum of the 11360—*Brown-red slate* sample only showed a distinguishable band at 287 cm^{-1} due to hematite, in addition to a series of broad bands falling within the 1130–1500 cm^{-1} range whose attribution remains doubtful.

Similarly, the portable Raman spectra collected on the synthetic (color index: PR101) iron oxide-based references (see Figure 3c) revealed, even in this case, an almost uniform composition based on iron(III) oxide–hematite according to the presence of the previously described modes. Some exceptions were recognized in the case of samples 40542 and 40545, respectively associated with *light* and *deep English red*, where a combination of hematite + gypsum and hematite + calcite was observed. Finally, with reference to the Hg-based pigments (11620—*Natural Cinnabar*, 11621—*Natural Cinnabar, light,* and 11622—*Natural Cinnabar, powder*), the portable Raman spectra (Figure 3d) revealed the three main contributions of vermilion, falling at 251 cm^{-1} (A_{1g}), 280 cm^{-1} (E_g), and 344 cm^{-1} (E_g), in compliance with the certified datasheet provided by the manufacturer. Noteworthy, the employment of a red laser enables the acquisition of the highest-quality Raman spectrum in the case of vermilion due to a close matching of the laser frequency with an electronic transition of such compound. Consequently, resonant, or pre-resonant, Raman scattering phenomena are likely to occur, significantly amplifying the Raman signal by a factor ranging from 10^2 to 10^6.

However, in the case of Carmine naccarat (ID code: 42100), Dragon's blood (ID code: 37000), Madder lake (ID code: 37202), Lac dye (ID code: 36020), and Resina kamala (ID code: 37030), the occurrence of a strong fluorescence background made the assessment of a reliable assignment difficult and, for this reason, their Raman signals will not be listed in the database. The same considerations can also be made for the pigment Burgundy red ochre deep 0–80 μ (ID code: 11576) and Burgundy red ochre deep 0–120 μ (ID code: 11577).

Concerning the vis-RS data, the SRF% curve reported in Figure 2b shows an increase for $\lambda > 550$ nm, typical of red-colored specimens, as expected. From a qualitative point of view, the behaviors of the SRF(%) profiles observed for the whole set were found to be slightly different from each other (See Figure 4), as it is known, they strongly depend on the specific properties of the pigment, including the particle size and crystal structure [76,77].

For pigments characterized by the same hue, the possibility to discern differences in their reflectance curves becomes challenging. In fact, the red pigments employed in this study show similar SRF(%) behavior characterized by the typical increase upon 550 nm < λ < 575 nm, with varying intensities. With the aim to provide further details, a first derivative calculation applied to the whole set of data was undertaken (see Supplementary Material (Figure S1)) for the assessment of the positions of the E.P.s characteristic of each red pigment. The set of E.P. positions for all the investigated red samples is listed in Table 3. An example is reported in Figure 2c, where the profile of d(SRF(%)) vs. λ is shown. The analysis of the d(SFR(%)) aids in identifying key wavelengths that contribute significantly to the hue of the pigment and mainly involves the identification of the most prominent maxima, accounting for the wavelength at which the pigment absorbs light mostly (λ_{p-h}). In the case of *Red jasper* (sample ID code 11300) the λ_{p-h} was found to be equal to 580 nm. A value of $\lambda_{p-h} = 580 \pm 10$ nm was also found for all the natural and synthetic iron oxide-based pigments, with the only exception being sample 52400—*translucent red medium* for which $\lambda_{p-h} = 600\ nm$. Higher values in the position of λ_{p-h} were found for all the organic-based red pigments (23610—*Alizarine crimson dark*, 42100—*carmine nacarat*, 37000—*Dragon's blood, powder*, 37202—*Madder lake*, 36020—*Lac dye,* and 37030—*Resina kamala*) ranging from 610 nm in the case of sample 42100—*carmine nacarat* to 640 nm for sample 37000—*Dragon's blood*.

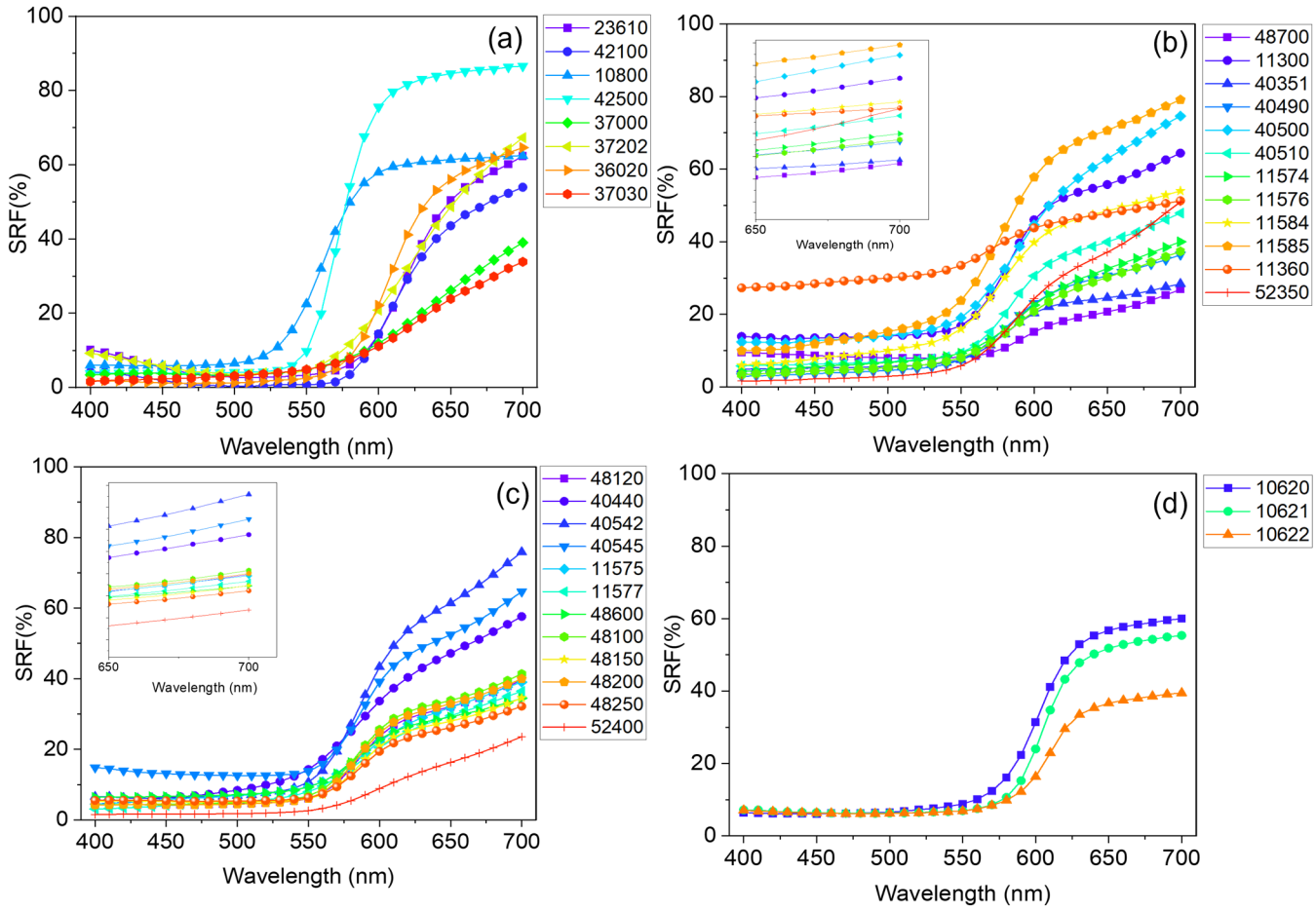

Figure 4. Spectral reflectance factor (SRF%) behavior of the 35 powdered samples reported in Table 3. Spectra were sorted into four different panels, respectively representative of (**a**) eight unique pigments respectively based on organic (23610—*Alizarine crimson dark*, 42100—*carmine nacarat*, 37000—*Dragon's blood, powder*, 37202—*Madder lake*, 36020—*Lac dye*, and 37030—*Resina kamala*), As- (10800—*Realgar*), and Pb-based compounds (42500—*Red lead, minium*), (**b**) natural (color index: PR102) and (**c**) synthetic (color index: PR101) iron oxide-based pigments, and (**d**) Hg-based ones.

A more detailed analysis allowed for the identification of relative maxima (λ_{p-l}), valleys (absolute/relative minima, λ_v), and shoulders (λ_{sh}), described in Section 2.2.1, whose assessment provides refined insights into the spectral behavior of each investigated pigment. Notably, the identification of such features in the d(SRF(%)) turns out to be crucial in the validation phase, as we will discuss in the following, in order to formulate hypotheses on the pigment color and production technique. In our example, an inspection of Figure 2c revealed the occurrence of two *valleys* and two *relative maxima*, respectively located at 420 and 640 nm, and 440 nm and 500 nm, together with a slight *shoulder*, concave in shape, located at 680 nm [78].

3.2. On-Site Measurement Results

Vis-RS and portable Raman spectra were collected from the 10 different red spots shown in Figure 1 and Table 2 (see points R#). The comparison of the obtained data with those present in the laboratory database helped validate the model and establish a reliable and efficient methodology for red pigment identification.

In Figure 5 the obtained portable Raman spectra (Figure 5a), SRF% trends (Figure 5b), and calculated first derivate curves (Figure 5c) are reported, the latter obtained only for five representative red pigmented areas, lighter and darker, respectively.

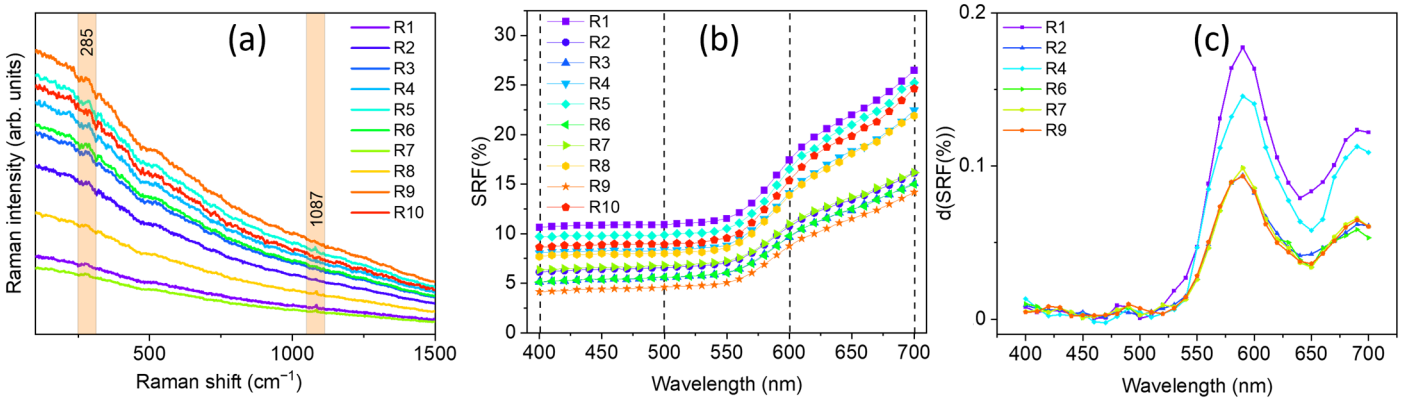

Figure 5. (**a**) Portable Raman spectra, (**b**) spectral reflectance factor (SRF%), and (**c**) calculated first derivate curves d(SRF(%)) (of five representative points for a feasible comparison) related to the red areas of the wall painting located at *The Norman Castle of Aci Castello*.

By looking at the collected portable Raman spectra, the presence of calcite ($CaCO_3$), from its main Raman contribution centered at 1086 cm^{-1}, can be identified in R1, R4, R5, R8, and R10. The detection of calcium carbonate should be attributed to the inherent chemical composition of the background layer. The primary constituent of this layer is a calcite-based compound grounded in the Italian '*fresco*' technique, in which pigments were applied directly on freshly laid mortar. However, the presence of calcite could be ascribed, other than to the background layer, to the possible use by the artist of a calcium carbonate-based white pigment, in a mixture with a pure red one, to obtain the desired lighter red hue observed by the naked eye in such areas (see Figure 1). Notably, in the case of the R2, R3, R6, R7, and R9 areas, no Raman signal at 1086 cm^{-1} can be distinguished.

Besides the presence of calcite, however, the high fluorescence background in the collected Raman spectra did not allow for the unambiguous identification of any other significant feature, except for a small signal around 285 cm^{-1} likely arising from the presence of iron oxides, making the identification of the red pigmenting a challenging task. In fact, from the database, a class of 14 different pigments display a Raman signature which can be comparable with those measured in situ. To overcome such limitation, a comparison of the d(SRF(%)) profiles, derived from the behavior of the corresponding spectral reflectance factor curves (Figure 5b,c), with those stored in the laboratory database allowed for the possibility to discriminate a set of 15 different red pigments with an absolute maximum in the d(SRF(%)) profile centered at 590 nm (p-h), i.e., pigment ID code: 48700, 48120, 40440, 40500, 40542, 40545, 11574, 11575, 11576, 11577, 48600, 48100, 48150, 48250, and 52350, well evident in the red areas of the wall painting.

To further refine the analysis, we compared the observed λ_{p-l}, λ_v, and λ_{sh} features in the d(SRF(%)) of Figure 5c with those associated with the previously identified 15 red pigments recorded in the database (see Table 3). An inspection of Figure 5c reveals, besides the absolute maximum at 590 nm ($\lambda_{p\text{-}h}$), a relative minimum around 470 nm, and two relative maxima at 490 nm and 690 nm. The correlation of the Raman profiles, which exhibit a comparable signature with such features in the d(SRF(%)), together with the position of the absolute maximum, allowed us to discriminate the employment of red ochre as a red pigmenting agent based on similarity criteria, according to the scheme of Figure 6.

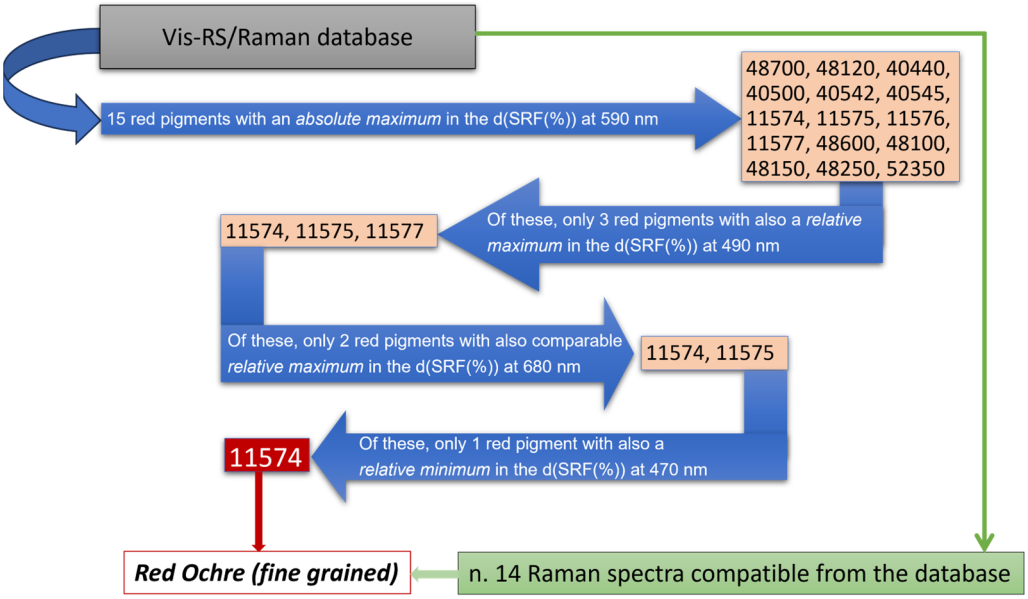

Figure 6. Flowchart utilized for the red pigment identification. Blue and green arrows refer, respectively, to vis-RS and portable Raman data.

In Figure 7, we report the comparison of the d(SRF(%)) vs. λ between R1, R2, R4, R6, R7, and R9 and sample ID code 11574.

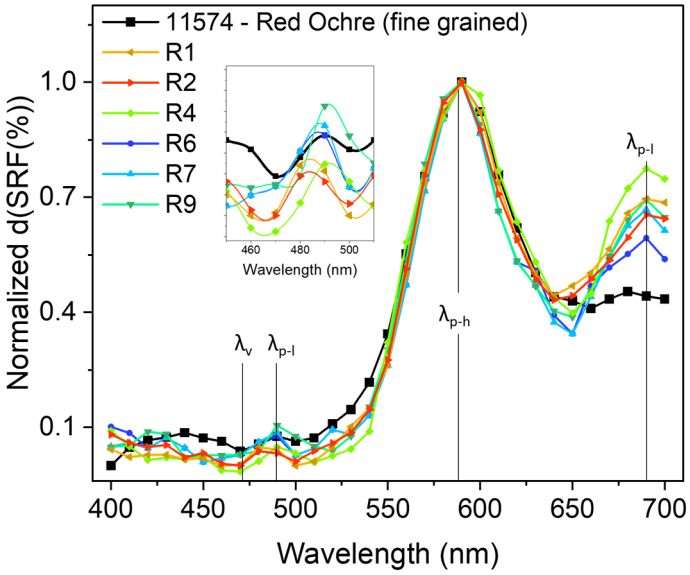

Figure 7. d(SRF(%)) vs. λ profiles related to the selected red areas and sample ID code 11574 (taken from the library), with the positions of the λ_{p-h}, $\lambda_{p-l,}$ and λ_v features indicated. All curves were normalized to the 590 nm absolute maximum value for a better comparison.

The presence of red ochre is supported by the fact that natural pigments were commonly used in wall painting from the Byzantine period to the Medieval one, sometimes associated with iron oxide.

It is worth noting that the aforementioned λ_{p-l} and λ_v features in the d(SRF(%)) curves represent more specific *smart markers* since they allow for the precise identification of a specific reference pigment which is otherwise not possible to uniquely accomplish from the absolute maximum at 590 nm (λ_{p-l}) or from the small signal around 285 cm^{-1} observed in the Raman profile. This is useful not only for pigment recognition, allowing us to overcome a series of limitations related to the use of portable Raman spectroscopy

as a single stand-alone approach, but also for making assumptions about the manufacturing technique. The fine-grained red ochre d(SRF(%)) profile (ID code: 11574) appears more compatible if compared, for example, to that of the coarse-grained red ochre (ID code: 11575).

4. Conclusions

In this work, we proposed a methodology for the accurate identification of red pigments used in historical–artistic contexts thanks to the evaluation of correlations that exist between vis-RS and portable Raman data, achieved through the employment of portable instrumentation. In particular, starting from the position of the Extrema Points (E.P.s) observed in the first derivative of the spectral reflectance factor (SRF%) curves and the Raman main vibrational signals collected for 35 pure red pigments supplied by ©*Kremer Pigmente*, a laboratory database was realized. The proposed database was then tested for the characterization of the red areas of a polychrome surface located within *The Norman Castle of Aci Castello* (Catania, Italy). As the main results, the comparison of the database data with those achieved in situ allowed us to discriminate, thanks to the identification of specific *smart markers*, the employment of fine-grained red ochre as a red pigmenting agent among a class of almost 15 different compatible pigments. In particular, it was shown that the identification of specific low-intensity features, i.e., relative maxima, relative minima, and shoulders in the d(SRF(%)) curves, which represent more specific *smart markers*, allowed us to validate the proposed procedure in cases in which ambiguous results can hinder a reliable pigment recognition.

Pigments of other hues will be analyzed and implemented in the database with the aim of verifying, in a more systematic manner, the proposed approach in different case studies.

Supplementary Materials: The following supporting information can be downloaded at: https://www.mdpi.com/article/10.3390/heritage7040102/s1, Figure S1: Profiles of the first derivative of spectral reflectance factor behavior of the 35 powdered samples reported in Table 1.

Author Contributions: Conceptualization, A.M.G., G.P. (Giuseppe Paladini), and G.S.; methodology, A.M.G., G.P. (Giuseppe Paladini), and G.S.; software, G.P. (Giuseppe Paladini) and G.S.; validation, E.P. and G.P. (Giuseppe Politi); formal analysis, G.P. (Giuseppe Paladini) and A.I.; investigation, R.G., G.P. (Giuseppe Paladini), and A.I.; resources, A.M.G. and G.S.; data curation, A.M.G., G.P. (Giuseppe Paladini), and G.S.; writing—original draft preparation, G.P. (Giuseppe Paladini), E.P., and G.S.; writing—review and editing, G.P. (Giuseppe Politi) and A.M.G.; visualization, A.M.G. and G.S.; supervision, A.M.G. and G.S.; project administration, G.S.; funding acquisition, A.M.G. All authors have read and agreed to the published version of the manuscript.

Funding: This research activity was funded by the European Union (NextGeneration EU), through the MUR-PNRR project SAMOTHRACE (ECS00000022).

Data Availability Statement: The data presented in this study are available on request from the corresponding author.

Acknowledgments: This research activity was funded by the European Union (NextGeneration EU), through the MUR-PNRR project SAMOTHRACE (ECS00000022) "SiciliAn MicronanOTecH Research And Innovation CEnter"–Ecosistema dell'innovazione (PNRR, Mission 4, Component 2 Investment 1.5, Avviso n. 3277 del 30-12-2021), Spoke 1–Università di Catania-Work Package 6 Cultural Heritage. The authors also wish to acknowledge the Aci Castello Municipality, the Ecomuseo Riviera dei Ciclopi, and, in particular, Major Carmelo Camillo Scandurra.

Conflicts of Interest: The authors declare no conflicts of interest.

References

1. Miguel, C.; Claro, A.; Gonçalves, A.P.; Muralha, V.S.F.; Melo, M.J. A study on red lead degradation in a medieval manuscript Lorvão Apocalypse (1189). *J. Raman Spectrosc.* **2009**, *40*, 1966–1973. https://doi.org/10.1002/jrs.2350.

2. Steger, S.; Stege, H.; Bretz, S.; Hahn, O. A complementary spectroscopic approach for the non-invasive in-situ identification of synthetic organic pigments in modern reverse paintings on glass (1913–1946). *J. Cult. Herit.* **2019**, *38*, 20–28. https://doi.org/10.1016/j.culher.2019.01.011.
3. Angelin, E.M.; Bacci, M.; Bartolozzi, G.; Cantisani, E.; Picollo, M. Contemporary artists' spinel pigments: Non-invasive characterization by means of electronic spectroscopy. *Spectrochim. Acta Part A Mol. Biomol. Spectrosc.* **2017**, *173*, 510–515. https://doi.org/10.1016/j.saa.2016.10.002.
4. Daniel Martin-Ramos, J.; Zafra-Gómez, A.; Vílchez, J.L. Non-destructive pigment characterization in the painting Little Madonna of Foligno by X-ray Powder Diffraction. *Microchem. J.* **2017**, *134*, 343–353. https://doi.org/10.1016/j.microc.2017.07.001.
5. Crupi, V.; La Russa, M.F.; Venuti, V.; Ruffolo, S.; Ricca, M.; Paladini, G.; Albini, R.; Macchia, A.; Denaro, L.; Birarda, G.; et al. A combined SR-based Raman and InfraRed investigation of pigmenting matter used in wall paintings: The San Gennaro and San Gaudioso Catacombs (Naples, Italy) case. *Eur. Phys. J. Plus* **2018**, *133*, 369. https://doi.org/10.1140/epjp/i2018-12231-7.
6. Venuti, V.; Fazzari, B.; Crupi, V.; Majolino, D.; Paladini, G.; Morabito, G.; Certo, G.; Lamberto, S.; Giacobbe, L. In situ diagnostic analysis of the XVIII century Madonna della Lettera panel painting (Messina, Italy). *Spectrochim. Acta Part A Mol. Biomol. Spectrosc.* **2020**, *228*, 117822. https://doi.org/10.1016/j.saa.2019.117822.
7. Pellis, G.; Bertasa, M.; Ricci, C.; Scarcella, A.; Croveri, P.; Poli, T.; Scalarone, D. A multi-analytical approach for precise identification of alkyd spray paints and for a better understanding of their ageing behaviour in graffiti and urban artworks. *J. Anal. Appl. Pyrolysis* **2022**, *165*, 105576. https://doi.org/10.1016/j.jaap.2022.105576.
8. Moura, L.; Melo, M.J.; Casanova, C.; Claro, A. A study on Portuguese manuscript illumination: The Charter of Vila Flor (Flower town), 1512. *J. Cult. Herit.* **2007**, *8*, 299–306. https://doi.org/10.1016/j.culher.2007.02.003.
9. Melo, M.J.; Claro, A. Bright Light: Microspectrofluorimetry for the Characterization of Lake Pigments and Dyes in Works of Art. *Acc. Chem. Res.* **2010**, *43*, 857–866. https://doi.org/10.1021/ar9001894.
10. Melo, M.J.; Otero, V.; Vitorino, T.; Araújo, R.; Muralha, V.S.F.; Lemos, A.; Picollo, M. A Spectroscopic Study of Brazilwood Paints in Medieval Books of Hours. *Appl. Spectrosc.* **2014**, *68*, 434–444. https://doi.org/10.1366/13-07253.
11. Longoni, M.; Bruni, S. Identification of Synthetic Organic Pigments in Contemporary Artists' Paints by FT-IR and FT-Raman: An Advanced Analytical Experiment. *J. Chem. Educ.* **2021**, *98*, 966–972. https://doi.org/10.1021/acs.jchemed.0c00875.
12. Liu, Y.; Lyu, S.; Hou, M.; Gao, Z.; Wang, W.; Zhou, X. A novel spectral matching approach for pigment: Spectral subsection identification considering ion absorption characteristics. *Remote Sens.* **2020**, *12*, 3415. https://doi.org/10.3390/rs12203415.
13. Kogou, S.; Lucian, A.; Bellesia, S.; Burgio, L.; Bailey, K.; Brooks, C.; Liang, H. A holistic multimodal approach to the non-invasive analysis of watercolour paintings. *Appl. Phys. A* **2015**, *121*, 999–1014. https://doi.org/10.1007/s00339-015-9425-4.
14. Eisnor, M.M.; McLeod, K.E.R.; Bindesri, S.; Svoboda, S.A.; Wustholz, K.L.; Brosseau, C.L. Electrochemical surface-enhanced Raman spectroscopy (EC-SERS): A tool for the identification of polyphenolic components in natural lake pigments. *Phys. Chem. Chem. Phys.* **2022**, *24*, 347–356. https://doi.org/10.1039/D1CP03301H.
15. Gueli, A.M.; Pasquale, S.; Politi, G.; Stella, G. The Role of Scale Adjustment in Color Change Evaluation. *Instruments* **2019**, *3*, 42. https://doi.org/10.3390/instruments3030042.
16. Pasquale, S.; Zimbone, M.; Ruffino, F.; Stella, G.; Gueli, A.M. Evaluation of the Photocatalytic Activity of Water-Based TiO2 Nanoparticle Dispersions Applied on Historical Painting Surfaces. *Heritage* **2021**, *4*, 1854–1867. https://doi.org/10.3390/heritage4030104.
17. D'Amico, S.; Comite, V.; Paladini, G.; Ricca, M.; Colica, E.; Galone, L.; Guido, S.; Mantella, G.; Crupi, V.; Majolino, D.; et al. Multitechnique diagnostic analysis and 3D surveying prior to the restoration of St. Michael defeating Evil painting by Mattia Preti. *Environ. Sci. Pollut. Res.* **2022**, *29*, 29478–29497. https://doi.org/10.1007/s11356-021-15880-5.
18. Andreotti, A.; Izzo, F.C.; Bonaduce, I. Archaeometric Study of the Mural Paintings by Saturnino Gatti and Workshop in the Church of San Panfilo, Tornimparte (AQ): The Study of Organic Materials in Original and Restored Areas. *Appl. Sci.* **2023**, *13*, 7153. https://doi.org/10.3390/app13127153.
19. Armetta, F.; Giuffrida, D.; Ponterio, R.C.; Falcon Martinez, M.F.; Briani, F.; Pecchioni, E.; Santo, A.P.; Ciaramitaro, V.C.; Saladino, M.L. Looking for the original materials and evidence of restoration at the Vault of the San Panfilo Church in Tornimparte (AQ). *Appl. Sci.* **2023**, *13*, 7088.
20. Colantonio, C.; Pelosi, C.; Calabrò, G.; Spizzichino, V.; Partenzi, I.; Lanteri, L. Scientific Investigation of Contemporary Pastel Painting by Roberto Sebastian Matta: Characterization of Original Materials through Multispectral Imaging and Spectroscopic Techniques. *Heritage* **2023**, *6*, 2541–2558. https://doi.org/10.3390/heritage6030134.
21. Iwanicka, M.; Moretti, P.; Pilz, K.; Doherty, B.; Cartechini, L.; Geldof, M.; de Groot, S.; Miliani, C.; Targowski, P. Congregation leaving the Reformed Church in Nuenen by Vincent van Gogh: A combined multi-instrumental approach to analyse the painting's stratigraphy in support of varnish removal. *Herit. Sci.* **2022**, *10*, 167. https://doi.org/10.1186/s40494-022-00789-0.
22. Pagnin, L.; Brunnbauer, L.; Wiesinger, R.; Limbeck, A.; Schreiner, M. Multivariate analysis and laser-induced breakdown spectroscopy (LIBS): A new approach for the spatially resolved classification of modern art materials. *Anal. Bioanal. Chem.* **2020**, *412*, 3187–3198. https://doi.org/10.1007/s00216-020-02574-z.
23. Lama, E.; Prieto-Taboada, N.; Etxebarria, I.; Bermejo, J.; Castro, K.; Arana, G.; Rodríguez Laso, M.D.; Madariaga, J.M. Spectroscopic characterization of xx century mural paintings of punta begoña's galleries under conservation works. *Microchem. J.* **2021**, *168*, 106423. https://doi.org/10.1016/j.microc.2021.106423.

24. Germinario, G.; Talarico, F.; Torre, M. Microanalyses and Spectroscopic Techniques for the Identification of Pigments and Pictorial Materials in Monet's Pink Water Lilies Painting. *Microsc. Microanal.* **2022**, *28*, 27–41. https://doi.org/10.1017/S1431927621013556.
25. Pappalardo, G.; Costa, E.; Marchetta, C.; Pappalardo, L.; Romano, F.P.; Zucchiatti, A.; Prati, P.; Mandò, P.A.; Migliori, A.; Palombo, L.; et al. Non-destructive characterization of Della Robbia sculptures at the Bargello museum in Florence by the combined use of PIXE and XRF portable systems. *J. Cult. Herit.* **2004**, *5*, 183–188. https://doi.org/10.1016/j.culher.2003.08.002.
26. Vandenabeele, P.; Castro, K.; Hargreaves, M.; Moens, L.; Madariaga, J.M.; Edwards, H.G.M. Comparative study of mobile Raman instrumentation for art analysis. *Anal. Chim. Acta* **2007**, *588*, 108–116. https://doi.org/10.1016/j.aca.2007.01.082.
27. Angelini, E.; Grassini, S.; Corbellini, S.; Ingo, G.M.; de Caro, T.; Plescia, P.; Riccucci, C.; Bianco, A.; Agostini, S. Potentialities of XRF and EIS portable instruments for the characterisation of ancient artefacts. *Appl. Phys. A* **2006**, *83*, 643–649. https://doi.org/10.1007/s00339-006-3546-8.
28. Perez-Alonso, M.; Castro, K.; Martinez-Arkarazo, I.; Angulo, M.; Olazabal, M.A.; Madariaga, J.M. Analysis of bulk and inorganic degradation products of stones, mortars and wall paintings by portable Raman microprobe spectroscopy. *Anal. Bioanal. Chem.* **2004**, *379*, 42–50. https://doi.org/10.1007/s00216-004-2496-2.
29. Casadio, F.; Toniolo, L. The analysis of polychrome works of art: 40 years of infrared spectroscopic investigations. *J. Cult. Herit.* **2001**, *2*, 71–78. https://doi.org/10.1016/S1296-2074(01)01107-4.
30. Leona, M.; Casadio, F.; Bacci, M.; Picollo, M. Identification of the Pre-Columbian Pigment Mayablue on Works of Art by Noninvasive UV-Vis and Raman Spectroscopic Techniques. *J. Am. Inst. Conserv.* **2004**, *43*, 39–54. https://doi.org/10.1179/019713604806112632.
31. Delaney, J.K.; Ricciardi, P.; Glinsman, L.D.; Facini, M.; Thoury, M.; Palmer, M.; Rie, E.R. de la Use of imaging spectroscopy, fiber optic reflectance spectroscopy, and X-ray fluorescence to map and identify pigments in illuminated manuscripts. *Stud. Conserv.* **2014**, *59*, 91–101. https://doi.org/10.1179/2047058412Y.0000000078.
32. Bonizzoni, L.; Bruni, S.; Gargano, M.; Guglielmi, V.; Zaffino, C.; Pezzotta, A.; Pilato, A.; Auricchio, T.; Delvaux, L.; Ludwig, N. Use of integrated non-invasive analyses for pigment characterization and indirect dating of old restorations on one Egyptian coffin of the XXI dynasty. *Microchem. J.* **2018**, *138*, 122–131. https://doi.org/10.1016/j.microc.2018.01.002.
33. Sfarra, S.; Ibarra-Castanedo, C.; Tortora, M.; Arrizza, L.; Cerichelli, G.; Nardi, I.; Maldague, X. Diagnostics of wall paintings: A smart and reliable approach. *J. Cult. Herit.* **2016**, *18*, 229–241. https://doi.org/10.1016/j.culher.2015.07.011.
34. D'Amico, S.; Venuti, V.; Colica, E.; Crupi, V.; Majolino, D.; Paladini, G.; Guido, S.; Mantella, G.; Zumbo, R. Scientific investigation of the Conversion of St Paul painting (Mdina, Malta). In Proceedings of the 2019 IMEKO TC4 International Conference on Metrology for Archaeology and Cultural Heritage, Florence, Italy, 4–6 December 2019; 2019; pp. 330–334.
35. Barone, G.; Crupi, V.; Longo, F.; Majolino, D.; Mazzoleni, P.; Raneri, S.; Venuti, V. A multi-technique approach for the characterization of decorative stones and non-destructive method for the discrimination of similar rocks. *X-Ray Spectrom.* **2014**, *43*, 83–92. https://doi.org/10.1002/xrs.2520.
36. Appolonia, L.; Vaudan, D.; Chatel, V.; Aceto, M.; Mirti, P. Combined use of FORS, XRF and Raman spectroscopy in the study of mural paintings in the Aosta Valley (Italy). *Anal. Bioanal. Chem.* **2009**, *395*, 2005–2013. https://doi.org/10.1007/s00216-009-3014-3.
37. Rosi, F.; Burnstock, A.; Van den Berg, K.J.; Miliani, C.; Brunetti, B.G.; Sgamellotti, A. A non-invasive XRF study supported by multivariate statistical analysis and reflectance FTIR to assess the composition of modern painting materials. *Spectrochim. Acta Part A Mol. Biomol. Spectrosc.* **2009**, *71*, 1655–1662. https://doi.org/10.1016/j.saa.2008.06.011.
38. de Faria, D.L.A.; Venâncio Silva, S.; de Oliveira, M.T. Raman microspectroscopy of some iron oxides and oxyhydroxides. *J. Raman Spectrosc.* **1997**, *28*, 873–878. https://doi.org/10.1002/(SICI)1097-4555(199711)28:11<873::AID-JRS177>3.0.CO;2-B.
39. Bacci, M.; Casini, A.; Cucci, C.; Picollo, M.; Radicati, B.; Vervat, M. Non-invasive spectroscopic measurements on the Il ritratto della figliastra by Giovanni Fattori: Identification of pigments and colourimetric analysis. *J. Cult. Herit.* **2003**, *4*, 329–336. https://doi.org/10.1016/j.culher.2003.09.003.
40. Plutino, A.; Richard, N.; Deborah, H.; Fernandez-Maloigne, C.; Ludwig, N.G. Spectral Divergence for Cultural Heritage applications. *Color Imaging Conf.* **2017**, *25*, 141–146. https://doi.org/10.2352/ISSN.2169-2629.2017.25.141.
41. Cavaleri, T.; Giovagnoli, A.; Nervo, M. Pigments and Mixtures Identification by Visible Reflectance Spectroscopy. *Procedia Chem.* **2013**, *8*, 45–54. https://doi.org/10.1016/j.proche.2013.03.007.
42. Dupuis, G.; Menu, M. Quantitative evaluation of pigment particles in organic layers by fibre-optics diffuse-reflectance spectroscopy. *Appl. Phys. A* **2005**, *80*, 667–673. https://doi.org/10.1007/s00339-004-3140-x.
43. Cosentino, A. Effects of different binders on technical photography and infrared reflectography of 54 historical pigments. *Int. J. Conserv. Sci.* **2015**, *6*, 287.
44. Gutiérrez-Neira, P.C.; Agulló-Rueda, F.; Climent-Font, A.; Garrido, C. Raman spectroscopy analysis of pigments on Diego Velázquez paintings. *Vib. Spectrosc.* **2013**, *69*, 13–20. https://doi.org/10.1016/j.vibspec.2013.09.007.
45. Briani, F.; Caridi, F.; Ferella, F.; Gueli, A.M.; Marchegiani, F.; Nisi, S.; Paladini, G.; Pecchioni, E.; Politi, G.; Santo, A.P.; et al. Multi-Technique Characterization of Painting Drawings of the Pictorial Cycle at the San Panfilo Church in Tornimparte (AQ). *Appl. Sci.* **2023**, *13*, 6492. https://doi.org/10.3390/app13116492.

46. de Waal, D. Raman investigation of ceramics from 16th and 17th century Portuguese shipwrecks. *J. Raman Spectrosc.* **2004**, *35*, 646–649. https://doi.org/10.1002/jrs.1210.
47. Striova, J.; Lofrumento, C.; Zoppi, A.; Castellucci, E.M. Prehistoric Anasazi ceramics studied by micro-Raman spectroscopy. *J. Raman Spectrosc.* **2006**, *37*, 1139–1145. https://doi.org/10.1002/jrs.1577.
48. Moioli, P.; Seccaroni, C. Analysis of Art Objects Using a Portable X-ray Fluorescence Spectrometer. *X-Ray Spectrom.* **2000**, *29*, 48–52. https://doi.org/10.1002/(SICI)1097-4539(200001/02)29:1<48::AID-XRS404>3.0.CO;2-H.
49. Mosca, S.; Frizzi, T.; Pontone, M.; Alberti, R.; Bombelli, L.; Capogrosso, V.; Nevin, A.; Valentini, G.; Comelli, D. Identification of pigments in different layers of illuminated manuscripts by X-ray fluorescence mapping and Raman spectroscopy. *Microchem. J.* **2016**, *124*, 775–784. https://doi.org/10.1016/j.microc.2015.10.038.
50. Muralha, V.S.F.; Miguel, C.; Melo, M.J. Micro-Raman study of Medieval Cistercian 12–13th century manuscripts: Santa Maria de Alcobaça, Portugal. *J. Raman Spectrosc.* **2012**, *43*, 1737–1746. https://doi.org/10.1002/jrs.4065.
51. Angelini, I.; Asscher, Y.; Secco, M.; Parisatto, M.; Artioli, G. The pigments of the frigidarium in the Sarno Baths, Pompeii: Identification, stratigraphy and weathering. *J. Cult. Herit.* **2019**, *40*, 309–316. https://doi.org/10.1016/j.culher.2019.04.021.
52. Guglielmi, V.; Comite, V.; Andreoli, M.; Demartin, F.; Lombardi, C.A.; Fermo, P. Pigments on Roman Wall Painting and Stucco Fragments from the Monte d'Oro Area (Rome): A Multi-Technique Approach. *Appl. Sci.* **2020**, *10*, 7121. https://doi.org/10.3390/app10207121.
53. Crocombe, R.A. Portable Spectroscopy. *Appl. Spectrosc.* **2018**, *72*, 1701–1751. https://doi.org/10.1177/0003702818809719.
54. Colomban, P. The on-site/remote Raman analysis with mobile instruments: A review of drawbacks and success in cultural heritage studies and other associated fields. *J. Raman Spectrosc.* **2012**, *43*, 1529–1535. https://doi.org/10.1002/jrs.4042.
55. Lauwers, D.; Hutado, A.G.; Tanevska, V.; Moens, L.; Bersani, D.; Vandenabeele, P. Characterisation of a portable Raman spectrometer for in situ analysis of art objects. *Spectrochim. Acta Part A Mol. Biomol. Spectrosc.* **2014**, *118*, 294–301. https://doi.org/10.1016/j.saa.2013.08.088.
56. Vandenabeele, P.; Edwards, H.G.M.; Jehlička, J. The role of mobile instrumentation in novel applications of Raman spectroscopy: Archaeometry, geosciences, and forensics. *Chem. Soc. Rev.* **2014**, *43*, 2628. https://doi.org/10.1039/c3cs60263j.
57. Vandenabeele, P.; Weis, T.L.; Grant, E.R.; Moens, L.J. A new instrument adapted to in situ Raman analysis of objects of art. *Anal. Bioanal. Chem.* **2004**, *379*, 137–142. https://doi.org/10.1007/s00216-004-2551-z.
58. Gueli, A.M.; Bonfiglio, G.; Pasquale, S.; Troja, S.O. Effect of particle size on pigments colour. *Color Res. Appl.* **2017**, *42*, 236–243. https://doi.org/10.1002/col.22062.
59. Gueli, A.M.; Pasquale, S.; Troja, S.O. Influence of vehicle on historical pigments colour. *Color Res. Appl.* **2017**, *42*, 823–835. https://doi.org/10.1002/col.22138.
60. Burrafato, G.; Troja, S..; Gueli, A.M.; Stella, G.; Zuccarello, A.. Ruolo della calibrazione nella valutazione delle varia-zioni cromatiche, Colore e Colorimetria contributi multidis-ciplinari. *Quad. Di Fotonica E Ottica* **2007**, *13*, 211–218.
61. Bacci, M.; Picollo, M.; Trumpy, G.; Tsukada, M.; Kunzelman, D. Non-Invasive Identification of White Pigments on 20Th-Century Oil Paintings by Using Fiber Optic Reflectance Spectroscopy. *J. Am. Inst. Conserv.* **2007**, *46*, 27–37. https://doi.org/10.1179/019713607806112413.
62. Montagner, C.; Bacci, M.; Bracci, S.; Freeman, R.; Picollo, M. Library of UV–Vis–NIR reflectance spectra of modern organic dyes from historic pattern-card coloured papers. *Spectrochim. Acta Part A Mol. Biomol. Spectrosc.* **2011**, *79*, 1669–1680. https://doi.org/10.1016/j.saa.2011.05.033.
63. Bacci, M.; Casini, A.; Picollo, M.; Radicati, B.; Stefani, L. Integrated non-invasive technologies for the diagnosis and conservation of the cultural heritage. *J. Neutron Res.* **2006**, *14*, 11–16. https://doi.org/10.1080/10238160600672930.
64. Liu, Z.; Zhang, H.; Zhou, W.; Hao, S.; Zhou, Z.; Qi, X.; Shi, J. Pigment identification on an undated Chinese painting by non-destructive analysis. *Vib. Spectrosc.* **2019**, *101*, 28–33. https://doi.org/10.1016/j.vibspec.2018.08.009.
65. Palamara, E.; Palles, D.; Kamitsos, E.I.; Pratim Das, P.; Tirado, J.I.; Nicolopoulos, S.; Zacharias, N. Fragments of luxury: Opaque glass from the Palace of Mystras, Greece. *J. Archaeol. Sci. Rep.* **2023**, *51*, 104145. https://doi.org/10.1016/j.jasrep.2023.104145.
66. Lin, C.H.; Chang, Y.F. Comparison and characterization of pigments and dyes by Raman spectroscopy. *Anal. Sci.* **2022**, *38*, 483–495. https://doi.org/10.2116/analsci.21SAR03.
67. Bell, I.M.; Clark, R.J.H.; Gibbs, P.J. Raman spectroscopic library of natural and synthetic pigments (pre- ≈ 1850 AD). *Spectrochim. Acta Part A Mol. Biomol. Spectrosc.* **1997**, *53*, 2159–2179. https://doi.org/10.1016/S1386-1425(97)00140-6.
68. Lafuente, B.; Downs, R.T.; Yang, H.; Stone, N. The power of databases: The RRUFF project. In *Highlights in Mineralogical Crystallography*; Armbruster, T., Danisi, R.M., Eds.; De Gruyter: Berlin, Germany, 2015; pp. 1–30. ISBN 9783110417104.
69. Baraldi, P.; Fagnano, C.; Ghittoni, A.L.; Tassi, L.; Zannini, P. Vibrational spectra of some pigments from Pompeii. *Acta Univ. Carol. Geol.* **2002**, *1*, 49–65. https://doi.org/10.1400/173336.
70. Baraldi, P.; Baraldi, C.; Curina, R.; Tassi, L.; Zannini, P. A micro-Raman archaeometric approach to Roman wall paintings. *Vib. Spectrosc.* **2007**, *43*, 420–426. https://doi.org/10.1016/j.vibspec.2006.04.029.
71. Bruni, S.; Cariati, F.; Consolandi, L.; Galli, A.; Guglielmi, V.; Ludwig, N.; Milazzo, M. Field and Laboratory Spectroscopic Methods for the Identification of Pigments in a Northern Italian Eleventh Century Fresco Cycle. *Appl. Spectrosc.* **2002**, *56*, 827–833. https://doi.org/10.1366/000370202760171482.

72. Amadori, M.L.; Poldi, G.; Germinario, G.; Arduini, J.; Mengacci, V. Spectroscopic and Imaging Analyses on Easel Paintings by Giovanni Santi. *Appl. Sci.* **2023**, *13*, 3581. https://doi.org/10.3390/app13063581.
73. Amadori, M.L.; Baraldi, P.; Barcelli, S.; Poldi, G. New Studies on Lorenzo Lotto ' S Pigments : Non-Invasive and Micro-Invasive Analyses. In *AI Ar. 2012 Modena, VII Congresso Nazionale di Archeometria, Atti del Congresso*; Pàtron Editore: Bologna, Italy, 2011.
74. IRUG. Keyword Search IRUG Spectral Database. Available online: http://www.irug.org/search-spectral-database (accessed on 10 November 2023).
75. RRUFF. Search RRUFF Sample Data. Available online: http://rruff.info/ (accessed on 10 November 2023).
76. Aceto, M.; Fenoglio, G.; Labate, M.; Picollo, M.; Bacci, M.; Agostino, A. A fast non-invasive method for preliminary authentication of mediaeval glass enamels using UV–visible–NIR diffuse reflectance spectrophotometry. *J. Cult. Herit.* **2020**, *45*, 33–40. https://doi.org/10.1016/j.culher.2020.05.003.
77. Elias, M.; Chartier, C.; Prévot, G.; Garay, H.; Vignaud, C. The colour of ochres explained by their composition. *Mater. Sci. Eng. B* **2006**, *127*, 70–80. https://doi.org/10.1016/j.mseb.2005.09.061.
78. Marey Mahmoud, H.H. Colorimetric and spectral reflectance access to some ancient Egyptian pigments. *J. Int. Colour Assoc.* **2019**, *24*, 35–45.